

THE SHAPES, ORIENTATION, AND ALIGNMENT OF GALACTIC DARK MATTER SUBHALOS

MICHAEL KUHLEN¹, JÜRIG DIEMAND^{2,4}, & PIERO MADAU^{2,3}¹School of Natural Sciences, Institute for Advanced Study, Einstein Lane, Princeton, NJ 08540²Department of Astronomy & Astrophysics, University of California, Santa Cruz, CA 95064³European Southern Observatory, Karl-Schwarzschild-Str. 2, D-85748 Garching, Germany⁴Hubble Fellow

ABSTRACT

We present a study of the shapes, orientations, and alignments of Galactic dark matter subhalos in the “Via Lactea” simulation of a Milky Way-size Λ CDM host halo. Whereas isolated dark matter halos tend to be prolate, subhalos are predominantly triaxial. Overall subhalos are more spherical than the host halo, with minor to major and intermediate to major axis ratios of 0.68 and 0.83, respectively. Like isolated halos, subhalos tend to be less spherical in their central regions. The principal axis ratios are independent of subhalo mass, when the shapes are measured within a physical scale like $r_{V_{\max}}$, the radius of the peak of the circular velocity curve. Subhalos tend to be slightly more spherical closer to the host halo center. The spatial distribution of the subhalos traces the prolate shape of the host halo when they are selected by the largest V_{\max} they ever had, i.e. before they experienced strong tidal mass loss. The subhalos’ orientation is not random: the major axis tends to align with the direction towards the host halo center. This alignment disappears for halos beyond $3r_{200}$ and is more pronounced when the shapes are measured in the outer regions of the subhalos. The radial alignment is preserved during a subhalo’s orbit and they become elongated during pericenter passage, indicating that the alignment is likely caused by the host halo’s tidal forces. These tidal interactions with the host halo act to make subhalos rounder over time.

Subject headings: cosmology: theory – dark matter – galaxies: dwarfs – galaxies: formation – galaxies: halos – methods: numerical

1. INTRODUCTION

Cold dark matter (CDM) halos are not smooth. Early numerical simulations of the formation of CDM halos lacked sufficient resolution to detect much besides the gross features of the mass distribution (Davis et al. 1985; Frenk et al. 1985; Quinn et al. 1986; Efstathiou et al. 1988; Frenk et al. 1988). Rapid advances in computational power and in the efficiency of codes have afforded a dramatic reduction in the particle masses and gravitational softening lengths. Multi-mass techniques (e.g. Katz & White 1993; Bertschinger 2001) allow even further resolution increases in particular areas of interest. The resulting high resolution maps of the matter distribution in CDM halos have revealed an astonishing abundance of substructure (Klypin et al. 1999; Moore et al. 1999; Diemand et al. 2007a, hereafter paper I). In “Via Lactea”, the most recent and highest resolution CDM simulation of a Galaxy scale halo to date, the total number of identifiable subhalos has reached $\sim 10,000$, which together account for 5.6% of the total host halo mass (paper I). Recent progress notwithstanding, the currently achievable mass resolution is orders of magnitude above the true cutoff in the CDM fluctuation power spectrum, and given the observed scale-invariant nature of the subhalo mass function ($dN/d\ln M \propto M^{-1}$), it is likely that the total substructure abundance and mass fraction has not yet converged.

CDM halos are not round. Whereas analytical work often treats CDM halos as spherically symmetric mass distributions, it has been known for some time (Barnes & Efstathiou 1987; Efstathiou et al. 1988; Frenk et al. 1988) that in general CDM halo shapes show significant departures from sphericity.

There is now a large body of work concerning the shapes of isolated CDM halos (Dubinski & Carlberg 1991; Katz 1991; Warren et al. 1992; Dubinski 1994; Jing et al. 1995; Tormen 1997; Thomas et al. 1998; Bullock 2002; Jing & Suto 2002; Springel et al. 2004; Bailin & Steinmetz 2005; Kasun & Evrard 2005; Hopkins et al. 2005; Allgood et al. 2006; Bett et al. 2007; Hayashi et al. 2007; Macciò et al. 2007) and widespread agreement on a number of findings: CDM halos tend to be prolate, they are more spherical in their outer regions, more massive halos tend to have smaller axis ratios, the moment of inertia is aligned with the shape velocity anisotropy tensor, the smallest principal axis tends to line up with the angular momentum vector, etc. (for a recent summary, see Allgood et al. 2006).

With Via Lactea’s unprecedented resolution, we are now for the first time able to extend this shape analysis to a well resolved subhalo population. This is interesting from a theoretical point of view, because of the important role that tidal interactions play in shaping the properties of the subhalo population. The shapes of subhalos are likely to be affected by tidal deformations, and a careful analysis of the subhalo shapes might allow us to better understand the tidal interactions.

Knowledge of subhalo shapes is important for several types of observational studies as well. Weak lensing is becoming a very valuable tool for probing cosmological parameters (Brown et al. 2003; Bacon et al. 2003; Hamana et al. 2003; Jarvis et al. 2003; Hoekstra et al. 2006; Massey et al. 2007) and constraining density profiles of galaxy groups and clusters (Brainerd 2004; Mandelbaum et al. 2006a). Any alignment between intrinsic galaxy ellipticity and with other galaxies or the

local mass density will introduce a bias into the lensing signal (Hirata & Seljak 2004; Bridle & King 2007). In fact, Lee et al. (2005) found evidence for an intrinsic alignment, with subhalo minor axes preferentially perpendicular to the host halo’s major axis, in a numerical simulation of four cluster scale halos, resolved with $\sim 2 \times 10^6$ particles each. They also developed an analytical model under the assumption that this alignment was caused by the host halo’s tidal field, and showed that it reproduces the numerical findings well. Observational evidence for subhalo alignment has been found in the Sloan Digital Sky Survey (SDSS), for galaxies in clusters (Agustsson & Brainerd 2006; Mandelbaum et al. 2006b) as well as in groups (Faltenbacher et al. 2007). Based on N-body numerical experiments Ciotti & Dutta (1994) concluded that the tidal field of a spherical cluster could be responsible for the observed radial alignment of cluster galaxy isophotes. A better understanding of typical subhalo shapes and their alignment within the host halo might allow a statistical correction of the resulting bias.

Another observational arena dependent on subhalo shapes are stellar kinematical studies of Local Group dwarf galaxies, which are being used to constrain the masses of their DM host halos (Wilkinson et al. 2004; Lokas et al. 2005; Muñoz et al. 2005; Walker et al. 2006; Gilmore et al. 2007; Strigari et al. 2007). In almost all cases the analysis is performed assuming spherical symmetry and often also a constant velocity anisotropy. More sophisticated analyses of the dwarf galaxy stellar motions will benefit from firm theoretical expectations of the intrinsic DM subhalo shapes and should result in more realistic models of the underlying DM mass distribution.

This paper is organized as follows. In Section 2 we briefly outline the technique we employed to determine the shape of subhalos. We present the shape parameters of the Via Lactea host halo in Section 3, and move on in Section 4 to discuss the dependence of the subhalo’s shape parameters on the radius at which they are measured, on their distance from the center of the host, and on the subhalo’s mass. In Section 5 we present results concerning the spatial distribution of the subhalos within the host halo and the alignment of their ellipsoids towards the host halo center. In Section 6 we consider the redshift evolution of the shapes of a sample of strongly tidally affected subhalos. Section 7 contains a discussion and summary of our results.

2. SIMULATION AND SHAPE FINDING METHOD

The main sample of subhalos analyzed in this work stems from the $z = 0$ output of the “Via Lactea” simulation (paper I). This simulation follows the dark matter substructure of a Milky-Way-scale halo ($M_{200} = 1.77 \times 10^{12} M_{\odot}$) with 234 million particles. With a particle mass of $\simeq 20,000 M_{\odot}$, the simulation resolves around 10,000 subhalos within $r_{200} = 388$ kpc. The global $z = 0$ properties of the host halo and the substructure population was presented in paper I and the joint temporal evolution of host halo and substructure properties, with an emphasis on tidal interactions, was discussed in Diemand et al. (2007b, hereafter paper II). Here we focus on the shapes of the matter distribution in Via Lactea’s host halo and subhalo population.

For the determination of (sub)halo shapes we follow

the iterative technique outlined in Allgood et al. (2006). This method is based on diagonalizing the weighted moment of inertia tensor

$$\tilde{I}_{ij} = \sum_n \frac{x_{i,n} x_{j,n}}{r_n^2}, \quad (1)$$

where

$$r_n = \sqrt{x_n^2 + (y_n/q)^2 + (z_n/s)^2} \quad (2)$$

is the ellipsoidal distance in the eigenvector coordinate system between the (sub)halo’s center and the n^{th} particle, and $q = b/a$ and $s = c/a$ are the intermediate-to-major and minor-to-major axis ratios, respectively ($a \geq b \geq c$). Initially \tilde{I}_{ij} is calculated for all particles within a spherical window of radius r_0 . In subsequent iterations we fix $a = r_0$ and include only particles with $r_n < r_0$. Iteration continues until q and s change by less than 10^{-3} . The degree of triaxiality of a halo is quantified by the triaxiality parameter introduced by Franx et al. (1991)

$$T = \frac{1 - q^2}{1 - s^2}. \quad (3)$$

A halo is said to be oblate for $T < 1/3$, triaxial for $1/3 < T < 2/3$, and prolate for $T > 2/3$.

For comparison with observational data it is often more desirable to constrain the shape of the potential than the shape of the density distribution. The potential shape has the additional advantage that it is less sensitive to local density variations (from substructure for example) and is typically smooth and well approximated by concentric ellipsoids (Springel et al. 2004; Hayashi et al. 2007). Instead of measuring the potential shape directly, or by fitting ellipses to the intersections of isopotential surfaces with three orthogonal planes (as advocated by Springel et al. 2004), we diagonalize the unweighted kinetic energy tensor

$$K_{ij} = \frac{1}{2} \sum_n v_{i,n} v_{j,n}, \quad (4)$$

where the $v_{i,n}$ are measured in the restframe of the subhalo under consideration. K_{ij} is related to the potential energy tensor $W_{ij} = \sum x_i d\Phi/dx_j$ through the tensor virial theorem

$$\frac{1}{2} \frac{d^2 I_{ij}}{dt^2} = 2K_{ij} + W_{ij}. \quad (5)$$

The internal structure of the Via Lactea host halo remains practically unchanged after $z = 1.7$ (paper II) and we expect $d^2 I_{ij}/dt^2 = 0$ at $z = 0$. In that case the eigenvectors of K_{ij} should reflect the principal axes of the potential ellipsoid. Note that the assumption of a constant I_{ij} is likely to fail for subhalos that are being tidally stripped, and in this case the principal axes of K_{ij} will not necessarily reflect the shape of the potential. Instead of the iterative procedure applied for I_{ij} , we simply diagonalize K_{ij} for all particles within the moment of inertia ellipsoid at a given radius. In the following we will refer to shapes determined by diagonalization of I_{ij} and K_{ij} as the *mass* and *potential* shapes, respectively.

3. HOST HALO SHAPE

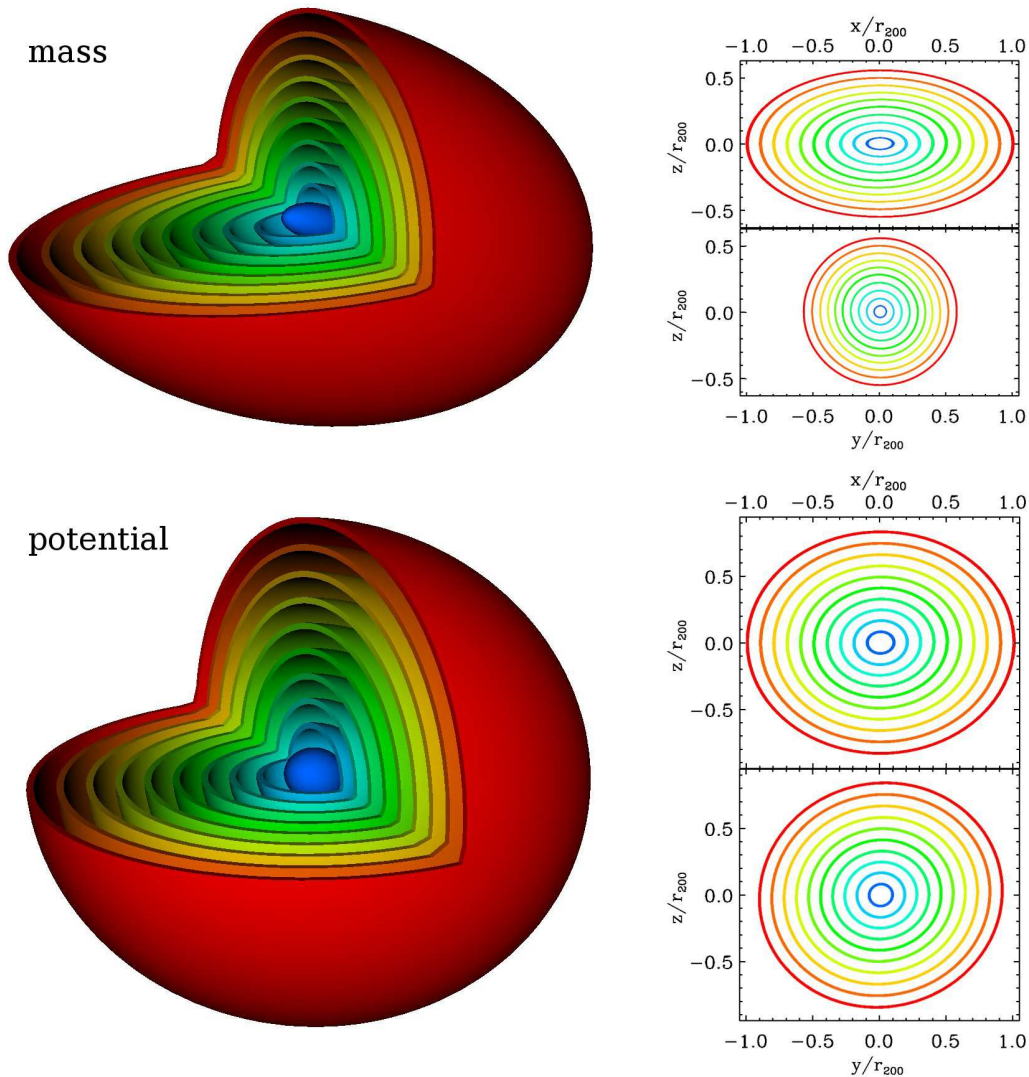


FIG. 1.— The shape of the Via Lactea halo as a function of radius, derived from diagonalizing the moment of inertia tensor I_{ij} (*top*), and the velocity anisotropy tensor K_{ij} as a proxy for the shape of the potential (*bottom*). The color indicates radius. The major principal axes at different radii are aligned to within 1° , and the mass and potential shapes are aligned to within 5° .

At the present epoch the Via Lactea host halo is prolate. We have determined the principal components of I_{ij} and K_{ij} as a function of major axis radius. The resulting shape ellipsoids are depicted in Fig. 1. Neither the shape nor the orientation of the ellipsoids vary much out to r_{200} . As a function of radius the major axis eigenvectors for both mass and potential shape are aligned to within 1° . As expected the potential is significantly rounder than the mass distribution, and the major axes of the two are aligned to within 5° at all radii. In Fig. 2 we plot mass and potential shape parameters q and s and triaxiality parameter T at $z=0, 0.5$, and 1 as a function of radius. Recall (from paper II, Figs. 3 and 4) that the spherically averaged mass distribution of the Via Lactea host halo remains remarkably constant *in proper coordinates* after the last major merger at $z = 1.7$ until today. We now see, however, that the host halo does undergo some adjustments in its shape.

At $z = 0$ the mass distribution becomes slightly less spherical towards the center with axis ratios dropping from ~ 0.55 at $200 \text{ kpc} < r < r_{200}$ to ~ 0.45 at 20 kpc,

whereas the potential shape axis ratios remains constant at around 0.8. The triaxiality parameter remains firmly in the prolate regime ($> 2/3$) for both mass and potential throughout the entire halo. The potential shape becomes slightly more prolate in the inner regions. At earlier times, however, we detect some significant changes in the axis ratios, especially in the outer regions. At $z = 0.5$ both q and s are larger by about 0.1-0.15 beyond 100 kpc, and at $z = 1$ q is significantly larger than s , resulting in a triaxial, as opposed to prolate, outer region beyond ~ 200 kpc. The potential shape exhibits variations of comparable magnitude. Note that the host halo accretes some fairly massive subhalos ($M_{\text{sub}}/M_{\text{host}} \sim 0.1$) between $z = 1$ and $z = 0.5$. Dynamical friction causes these subhalos to spiral in to the center over a few orbits, and they lose most of their mass ($> 99\%$) in this process. The associated redistribution of material probably contributes to the observed shape adjustments.

The shape of the Via Lactea host halo is consistent with previous studies of the shapes of dark matter halos, which have generally found them to be mostly prolate

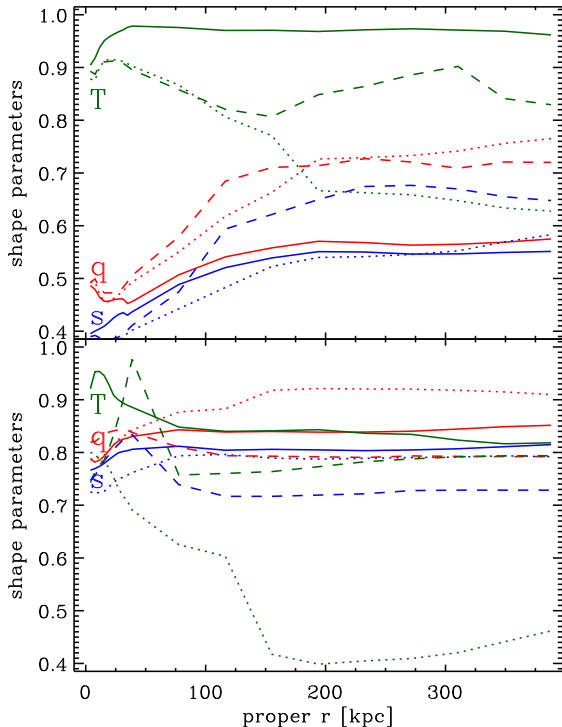


FIG. 2.— Host halo shape parameters for the mass distribution (*top panel*) and the potential (*bottom panel*) as a function of proper distance from the halo center at $z = 0$ (*solid lines*), $z = 0.5$ (*dashed lines*), and $z = 1$ (*dotted lines*). Intermediate to major axis ratio q (*red*), minor to major axis ratio s (*blue*), and triaxiality parameter T (*green*).

(e.g Allgood et al. 2006, and references therein). Observational studies of the shape of the Milky Way galaxy, however, have been much less conclusive. Disk warping (Olling & Merrifield 2000) and some models of the Sagittarius tidal stream (Ibata et al. 2001; Majewski et al. 2003; Martínez-Delgado et al. 2004) suggest that the Milky Way halo is close to spherical ($q \approx s \gtrsim 0.8$) and oblate, whereas some studies of the leading arm of the Sagittarius stream favor a prolate shape with $s = 0.6$ (Helmi 2004; Law et al. 2005).

The collisionless nature of our Via Lactea simulation prohibits a direct comparison between our findings and the observational constraints on the shape of the Milky Way host halo. Previous hydrodynamical numerical studies of galaxy formation have found that the cooling of baryons leads to significantly rounder halos (Kazantzidis et al. 2004; Springel et al. 2004; Bailin & Steinmetz 2005), especially in the central regions where s can increase by as much as 0.2 to 0.3. At the moment it is unclear how much of this effect is due to a potential overcooling problem in these simulations.

4. SUBHALO SHAPES

We now turn to the analysis of the shapes of Via Lactea’s subhalos. Unlike the host halo, which is resolved by over ten million particles even within $0.1r_{200}$, the subhalo shape determination is limited by numerical resolution. We restrict our analysis to halos containing at least 5,000 particles within their tidal radius, r_t . As in paper I, we define r_t as the point where the subhalo’s

spherically averaged density profile drops to twice the local underlying matter density. Via Lactea contains 97 such halos within r_{200} , 309 within $3r_{200}$, and 829 in total.

One complication arises from the difficulty in distinguishing between actual subhalo particles and those belonging to the underlying host halo. Our subhalo finder (6DFOF, cf. paper I) assigns all particles within the tidal radius to the subhalo, without removing unbound particles. Some contribution to I_{ij} and K_{ij} would thus come from background particles. This contribution is generally negligible for I_{ij} , since the background particles are more or less uniformly distributed throughout the subhalo. The host halo particles, however, significantly distort K_{ij} , because their velocities are typically much larger and more anisotropic than the subhalo particle velocities, especially for subhalos close to the host halo center. For this reason we have cleaned the subhalos from background host halo particles by comparing the members of each subhalo to those of its progenitor in the penultimate simulation output at $z = 0.005$ (~ 68.5 Myr before $z = 0$), and retained only those particles that also appear within r_t at the earlier time. This effectively removes all host halo particles from the subhalo and allows an accurate determination of K_{ij} . We have confirmed that the shape of I_{ij} is not affected by this cleaning procedure.

The subhalo tidal radius shrinks as subhalos pass through the inner regions of the host halo due to the increasing background density. However, as we showed in paper II, not all particles beyond this reduced r_t are actually stripped from the subhalo, and r_t re-expands as the subhalo begins its climb out of the host halo potential. Measuring the shape for all particles within the tidal radius thus probes more central regions for subhalos closer to the halo center than for subhalos in the outer regions. To avoid this bias we focus on the subhalo shapes for all particles within the radius of the peak of the circular velocity curve, $r_{V_{\max}}$. This choice comes at the cost of a reduced number of particles, but $r_{V_{\max}}$ does not temporarily decrease at pericenter passage.

4.1. Shape vs. Radius

We first discuss the dependence of subhalo shape on the radius at which they are measured, see Fig. 3. For this analysis we included the complete sample of 829 halos with more than 5000 particles within their tidal radius. Most of these halos currently lie outside of r_{200} , but a significant fraction (78% within $2r_{200}$) have passed through the host halo at some earlier time (paper II) and have experienced tidal interactions. Similarly to the Via Lactea host halo, we find that the subhalos’ mass distributions become slightly less spherical in the inner regions; $\langle q \rangle$ decreases from about 0.87 at $3r_{V_{\max}}$ to 0.68 at $0.2r_{V_{\max}}$, the innermost point at which we determine subhalo shapes. Similarly, $\langle s \rangle$ decreases from about 0.72 to about 0.45. The 68% scatter is about 0.2 for both q and s . As expected the potential shape shows even less dependence on radius and is almost spherical, with $\langle q \rangle \approx 0.9$ and $\langle s \rangle \approx 0.85$. The potential axis parameters also have a smaller 68% scatter of about 0.1.

Unlike isolated dark matter halos, which tend to be prolate, we find that subhalos are generally triaxial. $\langle T \rangle$ shows a slight decreasing trend with radius, but remains in the triaxial regime for both mass and potential shape

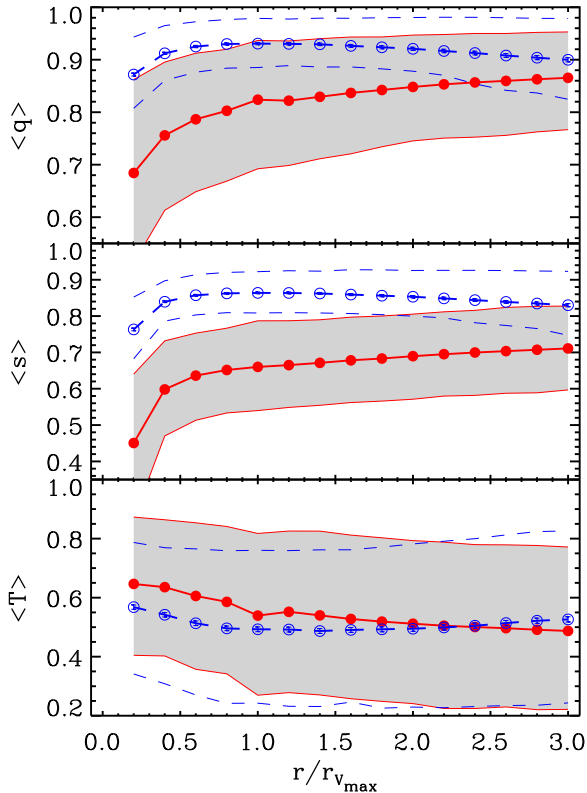


FIG. 3.— Mean (sub)halo shape parameters vs. the major axis radius of the ellipsoidal window used in the shape determination. We plot the shape of the moment of inertia tensor I_{ij} (solid lines, filled symbols) and the shape of the kinetic energy tensor K_{ij} (dashed lines, open symbols). The 68% scatter around the mean is indicated by the shaded region for I_{ij} and by the thin dashed lines for K_{ij} . Top panel: intermediate to major axis ratio, $q = b/a$. Middle panel: minor to major axis ratio $s = c/a$. Bottom panel: triaxiality parameter, $T = (1 - q^2)/(1 - s^2)$.

throughout the range of radii that we probed. Note that the 68% scatter around $\langle T \rangle$ extends into both the prolate and oblate regime. At $r_{V_{\max}}$ about 25% of all (sub)halos are prolate and an equal number oblate.

4.2. Shape vs. Distance

Next we take a look at the dependence of subhalo shapes on the distance from the halo center. For this purpose we use the shapes determined from all particles within $r_{V_{\max}}$. Fig. 4 shows that the shape of the mass distribution is close to independent of distance, with a weak but significant trend towards slightly larger axis ratios closer to the host halo center. Within r_{200} the mean axis ratios are $\langle q \rangle = 0.87$ and $\langle s \rangle = 0.74$, and outside of r_{200} they are $\langle q \rangle = 0.81$ and $\langle s \rangle = 0.64$. The potential shape is independent of distance, with $\langle q \rangle = 0.93$, $\langle s \rangle = 0.86$. The ellipsoids remains predominantly triaxial over the whole range of distance, for both mass and potential.

One might have expected a stronger distance dependence, since the subhalo shapes are affected by tidal interactions, which are stronger at the center. This is likely a consequence of measuring the shapes within $r_{V_{\max}}$, which is deep inside the halo mass distribution, and not as strongly affected by tides. Measuring the shapes within the tidal radius should give a more pronounced ef-

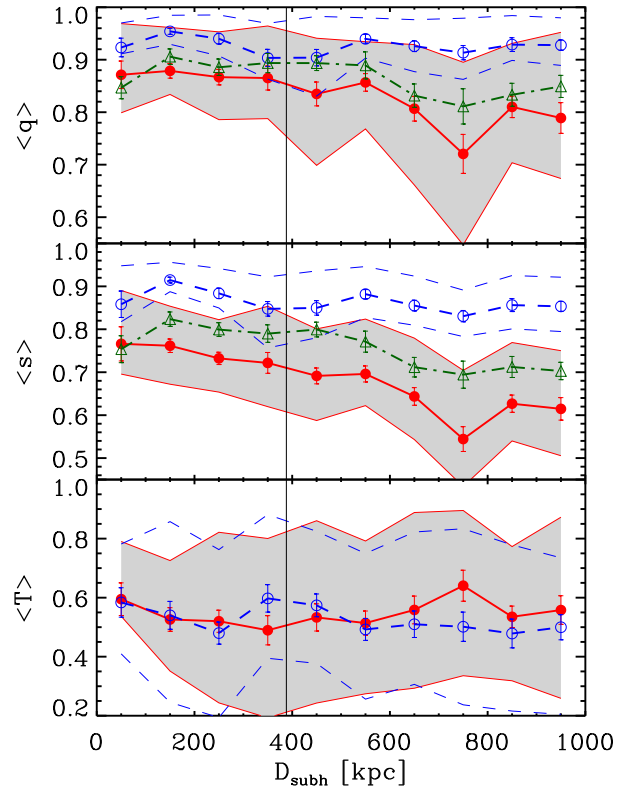


FIG. 4.— Mean (sub)halo shape parameters measured within $r_{V_{\max}}$ as a function of distance from the halo center. In addition to the mass shape (solid lines, filled circles) and the potential shape (dashed lines, open circles), in the top two panels we also plot the shape parameters measured within r_t (dash-dotted lines, open triangles). The thin solid line indicates $r_{200} = 388$ kpc.

fect, and indeed, when we look at the trend vs. distance for shapes measured within r_t (dashed lines and open triangles in Fig. 4) we find that for the innermost bin the mean axis ratios decrease. At least part of this trend, however, may also be explained by the temporary decrease of r_t as the subhalo passes through pericenter and the shape-radius dependence discussed in Section 4.1.

4.3. Shape vs. V_{\max}

Lastly, we consider the shape parameters as a function of the subhalo’s V_{\max} , a proxy for mass, Fig. 5. Again we use all 829 (sub)halos in the simulation. (Allgood et al. 2006) found that the axis ratios of isolated field halos measured at $0.3r_{\text{vir}}$ decreased with increasing halo mass, i.e. less massive halos are more spherical. In contrast, we find no such trend for subhalos. With the exception of the highest mass bin, both q and s appear to be independent of V_{\max} .

The highest V_{\max} bin (centered on 35 km s^{-1} , corresponding to a tidal mass of $\sim 10^{10} M_{\odot}$) has $\langle s \rangle = 0.57 \pm 0.05$, a bit less than would be expected from an extrapolation of the Allgood et al. (2006) $\langle s \rangle - M_{\text{halo}}$ relation which gives $\langle s \rangle \approx 0.69 \pm 0.04$ at $10^{10} M_{\odot}$ for $\sigma_8 = 0.74$. All but one of the six halos in this bin lie within $2r_{200}$ and can thus be considered subhalos. In Allgood et al. (2006) shapes were measured at $0.3r_{\text{vir}}$, whereas our subhalo shapes are measured at $r_{V_{\max}}$. We find it difficult to assign a “virial” radius to subhalos (paper II), and instead use the tidal radius r_t as the outer

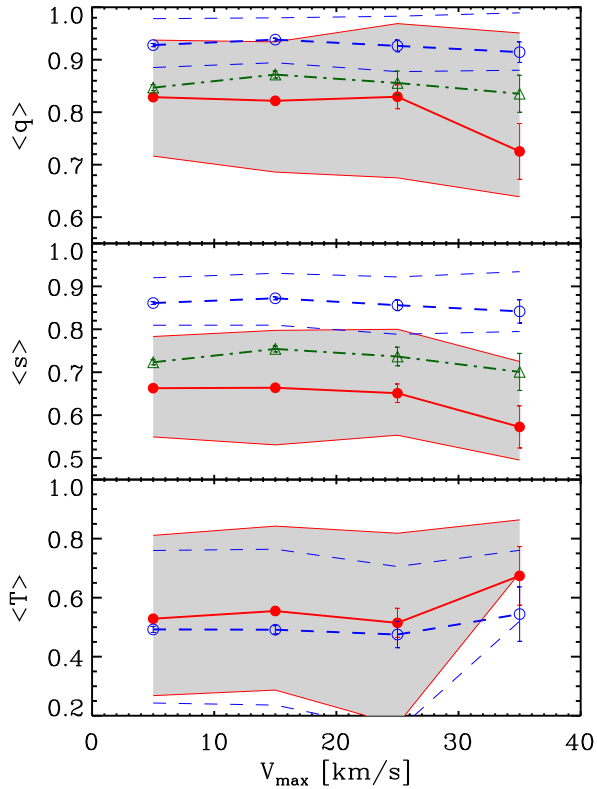


FIG. 5.— Subhalo shape parameters as a function of the subhalos peak circular velocity, a proxy for mass. Panels and symbols as in Fig. 4.

“edge” of the subhalo. The median ratio of $r_{V_{\max}}$ to r_t in this bin is 0.16, and for a $10^{10} M_{\odot}$ field halo with a concentration of $15 r_{V_{\max}}/r_{\text{vir}} = 2.163/c = 0.14$, so it is likely that we are simply measuring the shapes farther in, where axis ratios tend to be smaller (see Fig. 3). For comparison, $\langle s \rangle = 0.70$ when measured at r_t .

At any rate, our mean subhalo axis ratios become independent of mass at lower V_{\max} . It is possible that tidal interactions cause this flattening of the subhalo shape-mass relationship. Another possibility is that halo shapes (for both subhalos and field halos) are in fact intrinsically independent of mass when measured at a fixed physical scale, such as $r_{V_{\max}}$. In this case the mass dependence found at $0.3r_{\text{vir}}$ would in effect just be combination of radius dependence and the halo mass – concentration relation: $0.3r_{\text{vir}}$ is smaller than $r_{V_{\max}}$ in massive, low concentration halos. This means that relative to $r_{V_{\max}}$, the shapes of more massive halos are probed at smaller radii, where axis ratios tend to be smaller. Note that in this picture also the redshift dependence observed by Allgood et al. (2006) might in part be a consequence of a window ($0.3r_{\text{vir}}$) which becomes larger with time due to its co-moving definition. Further investigations will be necessary to fully address this issue.

5. SUBHALO DISTRIBUTION AND SHAPE ALIGNMENT

Having discussed the dependence of subhalo shapes on their properties, we now consider the spatial distribution and alignment within the host halo.

5.1. Spatial Distribution

TABLE 1
THE 3D SPATIAL DISTRIBUTION OF SUBHALOS

	N_h	q	s	θ_a	θ_b	θ_c
host halo	–	0.58	0.55	–	–	–
$M > 4 \times 10^6 M_{\odot}$	5404	0.66	0.54	10.1	36.2	34.7
$V_{\max} > 5 \text{ km s}^{-1}$	1571	0.68	0.58	13.5	20.1	15.9
$V_{\max,p} > 5 \text{ km s}^{-1}$	3824	0.64	0.59	8.36	15.1	12.8
$V_{\max,p} > 10 \text{ km s}^{-1}$	689	0.65	0.55	5.90	7.70	5.09
$V_{\max,p} > 15 \text{ km s}^{-1}$	224	0.64	0.52	10.6	3.13	10.9
top 100 $V_{\max,p}$	100	0.61	0.41	10.6	9.55	12.9
top 500 $V_{\max,p}$	500	0.67	0.54	4.47	4.42	2.91
top 1000 $V_{\max,p}$	1000	0.64	0.57	4.10	9.02	9.63

NOTE. — The shapes of the subhalo spatial distribution for different subhalo samples (described in the text). N_h is the number of subhalos in the sample, q and s the axis ratios, and $\theta_{a,b,c}$ the angle between the major, intermediate, and minor principal axis of the subhalo and the host halo ellipsoid.

The spatial distribution of subhalos depends sensitively on the sample selection criterion. In paper II we showed that the $z = 0$ distribution of Via Lactea subhalos is anti-biased compared to the mass distribution of the host halo. For subhalos selected to have a $z = 0$ mass greater than $4 \times 10^6 M_{\odot}$, the ratio of subhalo number density to host halo mass density is simply proportional to radius, whereas for subhalos selected to have a $z = 0$ V_{\max} greater than 5 km s^{-1} , this ratio scales as the enclosed mass. Previous studies have found that when subhalos are selected by their mass or V_{\max} at the time of accretion, this bias is substantially reduced, and the resulting subhalo number density profile more closely traces the underlying mass distribution (Nagai & Kravtsov 2005; Faltenbacher & Diemand 2006).

Here we extend this analysis to a full 3D spatial distribution of the subhalos. In addition to the two samples considered in paper II, we include a range of samples selected by the highest V_{\max} a subhalo reaches throughout its lifetime, a quantity we refer to as ‘ $V_{\max,p}$ ’. Three of these samples are defined by lower limits, $V_{\max,p} > 5, 10, \text{ and } 15 \text{ km s}^{-1}$, and three more by including the 100, 500, 1000 subhalos with the largest $V_{\max,p}$. This type of selection is designed to remove the bias introduced by tidal interactions, since the selection is performed on subhalo properties prior to their interaction with the host. For each sample of subhalos we diagonalize a weighted “moment of inertia” tensor (Eq.1) constructed from the $z = 0$ positions of the subhalos, without regard for their masses. We then calculate the axis ratios of the resulting ellipsoids and the angles between their principal axes and the principal axes of the host halo’s mass distribution measured at r_{200} .

The spatial distribution of all subhalo samples is triaxial, with s comparable to the underlying host halo density distribution and slightly larger q . Not all of the ellipsoids, however, are aligned with the host halo. The major axis of the ellipsoid defined by all subhalos with $M_t > 4 \times 10^6 M_{\odot}$ ($V_{\max} > 5 \text{ km s}^{-1}$) is tilted by 10.1° (13.5°) with respect to the host halo’s major axis. In general, the subhalo samples selected by $V_{\max,p}$ are more closely aligned with the host halo. The best alignment is found for the sample consisting of the 500 subhalos with the largest $V_{\max,p}$, whose principal axes are tilted by less than 5° from the host halo’s. The results for all samples are summarized in Table 1. Note that

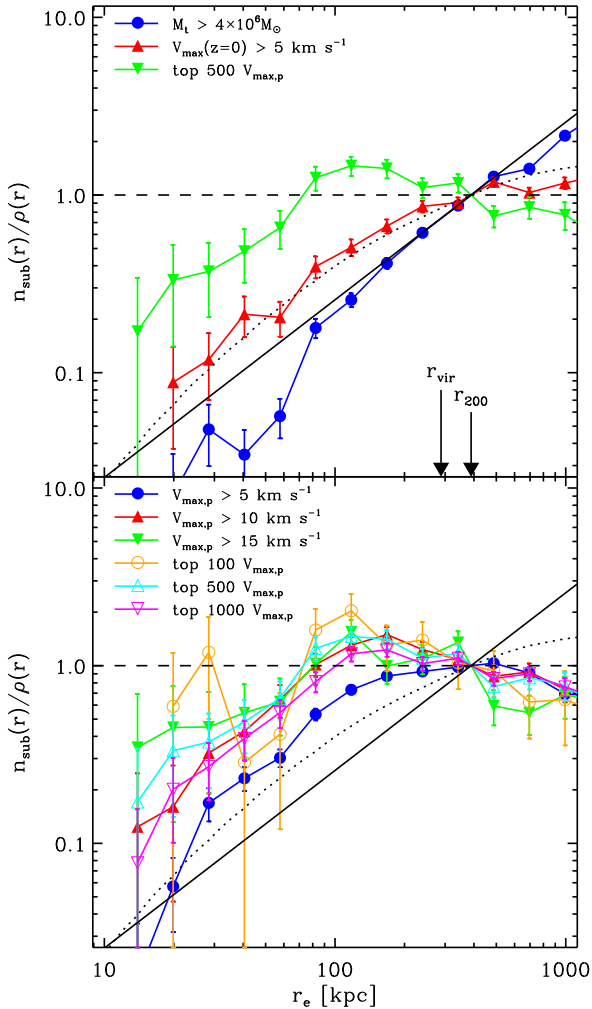


FIG. 6.— The ratio of the subhalo number density $n_{\text{sub}}(r_e)$ to the host halo mass density $\rho(r_e)$ as a function of ellipsoidal radius, $r_e = \sqrt{(x')^2 + (y'/q)^2 + (z'/s)^2}$. The ratio has been normalized to unity at $r_e = r_{200}$. The solid line indicates $n_{\text{sub}}/\rho \propto r$ and the dotted line $n_{\text{sub}}/\rho \propto M(<r)$.

Zentner et al. (2005), Libeskind et al. (2005, 2007), and Kang et al. (2007) also find that the substructure distribution is well aligned with the host halo orientation.

The radial dependence of the subhalo number density is presented in Fig. 6, where we plot the ratio of the subhalo number density to the host halo’s mass density as a function of r_e , the ellipsoidal radius (2). The ratio has been normalized to unity at $r_e = r_{200}$, in order to highlight the radial dependence in the interior of the host halo. The top panel clearly shows the radial dependence published in paper II hold also for ellipsoidal binning: subhalo samples selected according to their present mass or V_{max} are anti-biased with respect to the host halo mass distribution, with the former scaling as $n_{\text{sub}}/\rho \propto r$ down to ~ 60 kpc and the latter as $n_{\text{sub}}/\rho \propto M(<r)$ for the entire range of radii probed. The bottom panel shows that a selection based on $V_{\text{max,p}}$ removes a lot of this anti-bias. All six samples have a radial number density dependence closer to the host halo mass distribution than the samples selected according to $z = 0$ properties. The more restrictive the selection criterion is, the larger n_{sub}/ρ becomes. For some of the selections the ratio even exceeds unity from 80 kpc to r_{200} , indicating that these

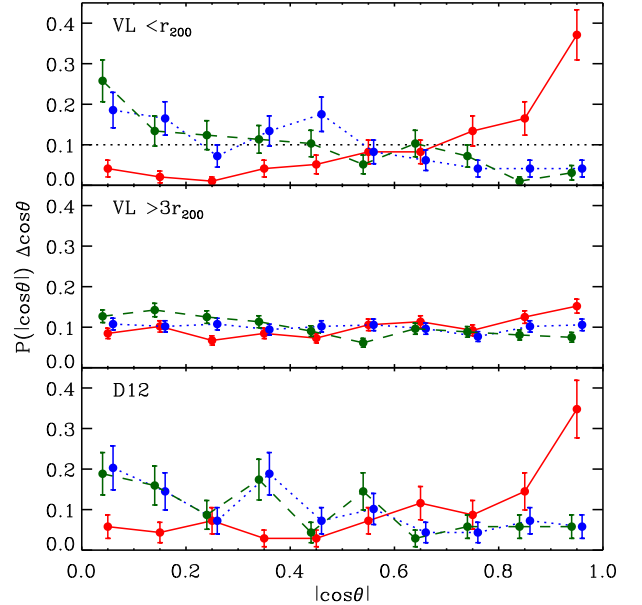


FIG. 7.— The distribution of the cosine of the angle between the direction towards the halo center and the subhalos’ major (solid lines), intermediate (dotted lines), and minor (dashed lines) axis, for all subhalos within r_{200} . The data points indicate the fraction of subhalos within each bin of width 0.1. *Top panel*: 97 Via Lactea subhalos within r_{200} . *Middle panel*: 520 Via Lactea subhalos outside of r_{200} . *Bottom panel*: 69 “D12” cluster subhalos within r_{vir} . The intermediate and minor axis data points have been offset by ± 0.01 in the horizontal direction for clarity.

samples are spatially biased with respect to the host halo, i.e. their abundances falls off with radius faster than the underlying density distribution. This bias is probably a consequence of dynamical friction. The subhalos with the largest $V_{\text{max,p}}$ were massive enough to experience some degree of dynamical friction and spiraled in towards the center. Along the way they lost mass, reducing the dynamical friction and preventing them from completely merging with the host. This process would preferentially remove such subhalos from the outer regions.

The “top 500 $V_{\text{max,p}}$ ” sample comes closest to tracing $\rho(r)$ (both in radial dependence and in the orientation of the shape ellipsoid), and we have plotted it in the top panel for direct comparison with the samples discussed in paper II. The decrease in n_{sub}/ρ below $r_e = 70$ kpc is probably at least partially due to numerical resolution, since the decrease is smaller for larger, and therefore better resolved subhalos.

5.2. Radial Alignment

Via Lactea’s very high numerical resolution allows us to investigate the orientation of dark matter subhalos with respect to the host halo center. We find strong evidence for preferential radial alignment of the subhalo triaxial mass distribution.

In the top panel of Fig. 7 we plot the distribution of $|\cos\theta|$, the absolute value of the cosine of the angle between each of the principal axes of the subhalo’s triaxial ellipsoid and the radius vector from the host halo center, for the 97 Via Lactea subhalos within r_{200} . If the subhalo ellipsoids were randomly distributed with respect to the halo center, this distribution would be flat. Instead we

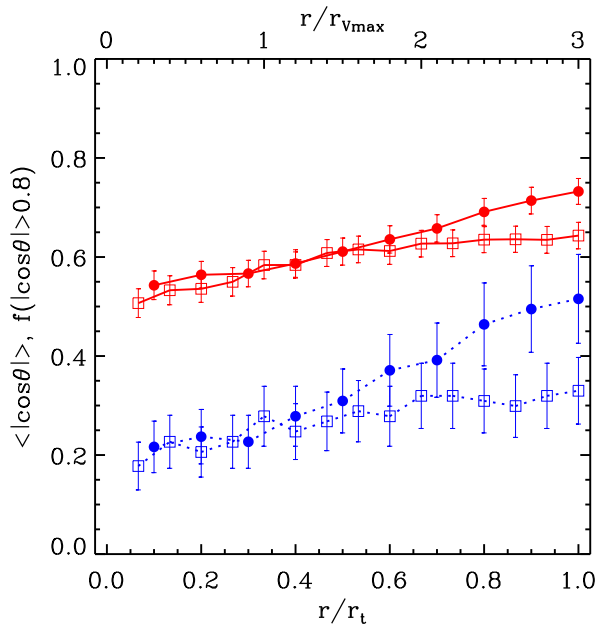


FIG. 8.— The dependence of the subhalo alignment towards the host halo center as function of subhalo radius at which the shape is measured. Only subhalos within r_{200} have been included. *Solid line*: the mean of $|\cos \theta|$ and its uncertainty. *Dotted line*: the fraction of subhalos with $|\cos \theta| > 0.8$ and its Poisson errors. Radii as a fraction of r_t (*filled circles*, lower axis) and as a fraction of $r_{V_{\max}}$ (*open squares*, upper axis).

see that the major axis distribution is strongly peaked towards large values of $|\cos \theta|$, indicating that the major axis preferentially points towards the halo center. Correspondingly, the intermediate and minor axes are biased towards low values of $|\cos \theta|$.

In the middle panel of Fig. 7 we plot the same distribution for all halos outside of $3r_{200}$. The distribution is flat, showing no evidence for alignment of any of the principal axes. The alignment effect appears to only be present for subhalos physically associated with the Via Lactea host halo, and this is one piece of evidence for a tidal origin of this radial alignment.

For comparison we have plotted (lower panel Fig. 7) the same distribution for the subhalos of a galaxy cluster scale dark matter halo, the 14 million particle “D12” cluster discussed in Diemand et al. (2004). The same subhalo shape alignment is present here too. Ragone-Figueroa & Plionis (2007) and Faltenbacher et al. (2007, in preparation) also observe such an alignment in a much larger sample of lower resolution group and cluster scale dark matter halos and their subhalo population.

If tidal interactions are indeed responsible for the radial alignment, then it may be expected that the alignment would be more pronounced in the outer regions of the subhalo, where tidal effects are strongest. Indeed we observe just such a trend when we look at the mean of $|\cos \theta|$ and $f(|\cos \theta| > 0.8)$, the fraction of subhalos with $|\cos \theta| > 0.8$, versus subhalo radius, see Fig. 8. For this analysis we restrict ourselves to subhalos within r_{200} , and consider radii as a fraction of both r_t and $r_{V_{\max}}$. When measured at r_t , about 55% of all subhalos have a major axis that is aligned to within 35° of the direction towards the halo center and $\langle |\cos \theta| \rangle = 0.75$. Both

$\langle |\cos \theta| \rangle$ and $f(|\cos \theta| > 0.8)$ decrease monotonically towards smaller r/r_t . The mean tidal radius for the 97 subhalos in this sample is $\langle r_t \rangle = 10.6$ kpc, and $\langle r_{V_{\max}} \rangle = 2.31$ kpc. Not surprisingly, the alignment signal is less pronounced when shapes are measured at $r_{V_{\max}}$. However, even in this case the alignment is significant: $\langle |\cos \theta| \rangle = 0.58$ with an uncertainty ($= \sqrt{\text{var}(|\cos \theta|)/N_{\text{sub}}}$) of 0.03, which corresponds to a $\sim 2.5\sigma$ significance.

Note that while Lee et al. (2005) finds that the subhalo minor axes are preferentially perpendicular to the host halo’s major axis in a study of cluster-scale subhalos, and Faltenbacher et al. (2007, in preparation) find a similar but weaker alignment signal in group-scale subhalos, we find no evidence for such an alignment in the Via Lactea subhalo population. The minor axes of our subhalo population shows no correlation with any of the host halo’s principal axes.

6. REDSHIFT EVOLUTION

The fact that the radial subhalo alignment is stronger for subhalos closer to the host halo center (see Fig. 7) and that the alignment signal is more pronounced when the shapes are measured in the outer regions of the subhalo (see Fig. 8) is suggestive of a tidal origin of the alignment. In this section we present additional support for this hypothesis by looking at the temporal evolution of the shapes and orientations of a small sample of subhalos, chosen according to the following criteria:

- i) the subhalos must lie within r_{200} at $z = 0$,
- ii) they must have undergone at least three pericenter passages since $z = 1.7$,
- iii) they must have experienced significant tidal mass loss, $\Delta M/M = 1.0 - M_t(z = 0)/M_t(z = 1.7) > 0.4$, and
- iv) they must contain more than 4000 particles at $z = 0$ ($M_t(z = 0) > 8 \times 10^7 M_\odot$).

These constraints result in a sample of 19 well resolved subhalos that have experienced significant tidal interactions with the host halo.

In Fig. 9 we show the temporal evolution of $\langle q \rangle$, $\langle s \rangle$, and $\langle V_{\max} \rangle$ for this subsample. The $\langle V_{\max} \rangle$ curve shows that these subhalos experience most of their mass growth early on and then continually lose mass due to tidal interactions with the host halo (see paper II for a more extensive discussion). Here we show that this tidal interaction also leads to subhalos becoming rounder with time. At formation they have $\langle q \rangle \approx 0.65$ and $\langle s \rangle \approx 0.5$, but these grow as they are captured and begin to feel the host halo’s tidal field. After $z = 1$ $\langle q \rangle$ remains stable at about 0.9, but $\langle s \rangle$ is still increasing slightly, reaching ~ 0.85 at $z = 0$. For comparison we also show the $z = 0$ mean axis ratios of the 520 halos outside of $3r_{200}$. Owing to their large distance from the host halo, these halos have experienced weaker tidal interactions. As expected these halos are less spherical than the tidally stripped sample: $\langle q \rangle = 0.85$ and $\langle s \rangle = 0.72$. This further supports the notion that tidal interactions tend to make subhalos rounder.

In the following we further restrict our sample, and look in more detail at the orbits of individual subhalos

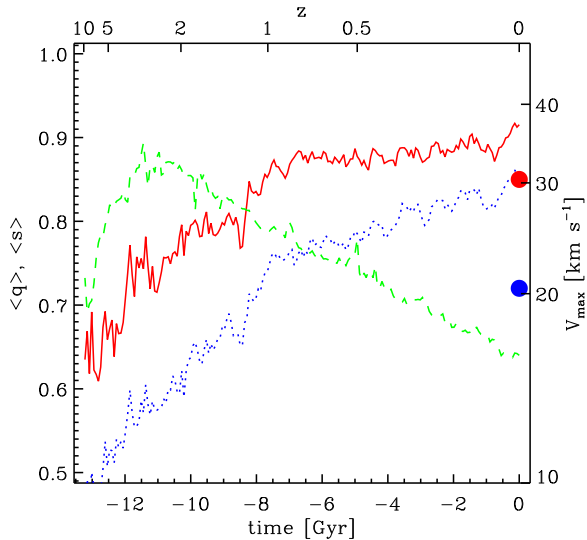


FIG. 9.— $\langle q \rangle$ (solid line, red), $\langle s \rangle$ (dotted line, blue), and V_{\max} (dashed line, green) for the 19 subhalo sample (see text for a discussion of their selection) as a function of time. The two filled circles at $z = 0$ indicate $\langle q \rangle$ and $\langle s \rangle$ for all halos beyond $3r_{200}$, which have been less affected by tides from the host halo. The shapes are determined within r_t .

and the time dependence of their shapes and alignments. For this purpose we hand selected five illustrative examples of subhalos with small pericenters ranging from 9.6 to 32 kpc. For comparison we also included one subhalo (Id #21500) with a higher angular momentum orbit and a pericenter of 69 kpc. The properties of the selected subhalos are summarized in Table 2.

In Fig. 10 we present a three-dimensional visualization of the orbits for the six subhalos in this sample. Starting with the $z = 0$ output and for every fourth output thereafter (corresponding to a time interval of 274 Myr) up to $z = 2$, we have plotted at the subhalo’s center of mass location an ellipsoid whose orientation and axis ratios are determined from all particles within the subhalo’s tidal radius. The major axis of each ellipsoid is indicated by a short solid line. For clarity we used a fixed major axis length of 10 kpc, although the tidal radii vary along the orbit. The orbits are shown in proper coordinates in the rest frame of the host halo and the sides of the box range from -300 to +300 kpc.

The most striking feature of these plots is that the radial alignment of the subhalo is preserved throughout the majority of its orbit. The subhalos’ ellipsoids perform a near perfect figure rotation such that the major axis continually points close to the host halo’s center. This figure rotation, however, is not seen in subhalo #21500, the one with the higher angular momentum orbit. Its orientation is almost independent of its orbital position.

We have quantified these trends in Fig. 11, where we plot each subhalo’s radius, its axis ratios q and s , and its $|\cos\theta|$ as a function of time. The evolution of q and s very closely tracks the orbit of the subhalo. Every time a subhalo passes through pericenter its axis ratios decrease. Note that part of this decrease can be attributed to the fact that the tidal radii shrink during pericenter passage, and so we are effectively measuring the subhalo shapes further in, where they are intrinsically less spher-

TABLE 2
SUBHALO PROPERTIES OF THE SHAPE EVOLUTION SUBSAMPLE

Subhalo Id	$z = 0$		$z = 1.7$		$\Delta M/M$
	M_t (M_\odot)	V_{\max} (km s^{-1})	M_t (M_\odot)	V_{\max} (km s^{-1})	
04242	2.4×10^8	15.4	3.7×10^9	28.2	0.93
10876	1.6×10^8	14.6	4.6×10^8	18.8	0.66
13351	4.4×10^8	18.8	2.6×10^9	66.9	0.84
13467	1.2×10^8	14.3	2.8×10^9	28.6	0.96
18412	1.3×10^8	12.5	4.0×10^9	32.5	0.97
21500	8.4×10^7	11.9	1.5×10^8	13.4	0.45

ical (see Section 4.1). However, r_t drops below $r_{V_{\max}}$ only for one or two outputs close to pericenter, and for most of the orbit remains in the regime where the axis ratios are almost independent of radius. Thus we conclude that the temporary decrease in r_t at pericenter is not sufficient to explain the full extent of the correlation between axis ratios and orbital position. Furthermore we see from the plot of $|\cos\theta|$ that the subhalos are indeed pointing close to the host halo center for the majority of their orbits. During the fast pericenter passages $|\cos\theta|$ drops significantly, but remains close to unity almost everywhere else. There are a few exceptions, where $|\cos\theta|$ drops below unity even away from pericenter, for example at $z = 0.7$ for #04242 and at $z = 0.4$ for #10876 and #13467, and these are most likely caused by close passages to other massive subhalos.

Together these trends provide strong evidence for a tidal origin of the radial alignment of subhalos. As they orbit the host halo’s center of mass, tidal forces continually distort the subhalos’ mass distribution, stretching them along the radial direction and compressing them in the perpendicular directions. This tidal distortion is stronger the closer the subhalo gets to the host halo center, but the pericenter passage occurs so quickly that the subhalo does not have enough time to adjust its orientation to point towards the center.

Our subsample, of course, was chosen to have experienced strong tidal interactions by requiring $\Delta M/M > 0.4$ and at least 3 pericenter passages. However, as we showed in paper II, more than half of all subhalos lose more than 50% of their mass from $z = 1$ to $z = 0$, and so tidally caused radial alignment is expected for most subhalos. As mentioned above, subhalo #21500 is one example of a subhalo that does not appear to experience much radial alignment. We found that of the 19 subhalos for which we performed a time dependent analysis, only three subhalos exhibit a similar lack of alignment-orbit correlation.

7. CONCLUSION

The main conclusions of this paper can be summarized in the following points.

- The shape of the Via Lactea host halo is prolate, and slightly less spherical (lower axis ratios) in the central regions. The shape of the potential ($q \approx s \approx 0.8$) is significantly rounder than the mass distribution ($q \approx s \approx 0.4 - 0.55$).
- Whereas isolated halos tend to be prolate, we find that subhalos are predominantly triaxial. Overall subhalos are more spherical than the host halo.

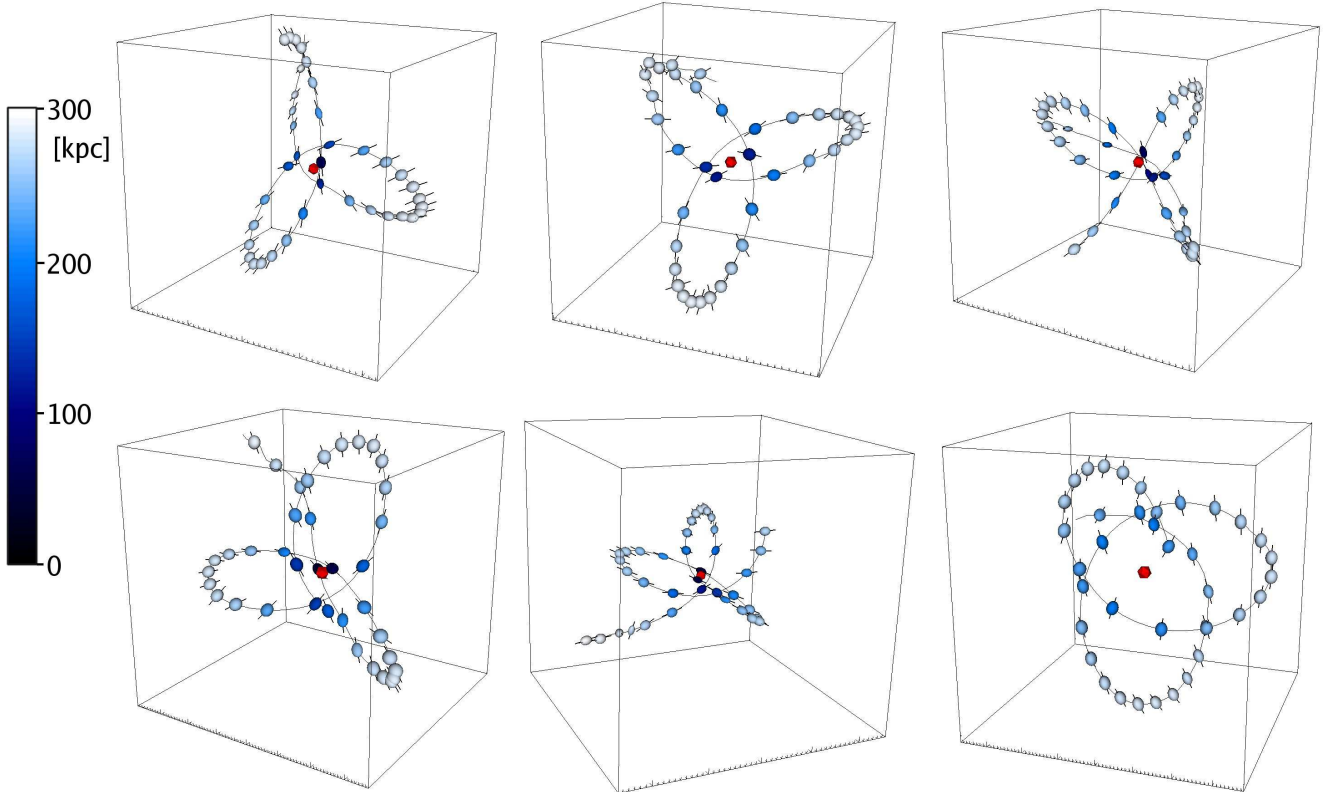


FIG. 10.— The proper space orbits and shapes of six subhalos (see text for a discussion of their selection) as function of time. Colors indicate the distance in proper kpc from the host halo center, which is indicated by the red icosahedron. The symbols depict ellipsoids of a constant size (major principal axis of 10 kpc) whose axis ratios and orientations are determined from all particles within the subhalo’s tidal radius. Ellipsoids are plotted for outputs between $z = 2$ and $z = 0$ with a stride of 4 outputs, corresponding to a time interval of 274 Myr. The major principal axes are indicated by short solid lines. The mass shape has $\langle q \rangle = 0.85$ and $\langle s \rangle = 0.68$, averaged over all subhalos within $3r_{200}$. The potential shape for these subhalos is very close to spherical, with $\langle q \rangle = 0.93$ and $\langle s \rangle = 0.86$. Like isolated halos, subhalos tend to be slightly less spherical in the central regions.

- We find a weak trend towards larger axis ratios for subhalos closer to the host halo center. Within r_{200} $\langle q \rangle = 0.87$ and $\langle s \rangle = 0.74$, compared with $\langle q \rangle = 0.82$ and $\langle s \rangle = 0.65$ for all subhalos outside of r_{200} .
- For subhalos with $V_{\max} < 30 \text{ km s}^{-1}$ the axis ratios are independent of V_{\max} . At higher V_{\max} they are slightly lower.
- The spatial distribution of subhalos matches the prolate shape of the host halo when subhalos are selected by $V_{\max,p}$, the largest V_{\max} they ever had during their lifetime. This type of selection also results in an ellipsoidal radius dependence of the subhalo abundance that more closely follows the mass distribution of the host halo than the anti-biased distributions from selections based on $z = 0$ subhalo properties like M_t and V_{\max} .
- The orientation of subhalo shape ellipsoids is not
- Tidal interactions with the host halo tend to make the subhalos rounder over time.
- For the majority of subhalos whose temporal evolution we studied here in detail, the radial alignment is preserved during the subhalo’s orbit, and the axis ratios decrease during pericenter passage. We conclude that the radial subhalo alignment is likely caused by tidal interactions with the host halo.

Support for this work was provided by NASA grants NAG5-11513 and NNG04GK85G. J.D. acknowledges support from NASA through Hubble Fellowship grant HST-HF-01194.01. The Via Lactea simulation was performed on NASA’s Project Columbia supercomputer system. The visualizations in Figs. 1 and 10 were created with VisIt (<http://www.llnl.gov/visit/>), a visualization tool developed by the DOE’s Advanced Simulation and Computing Initiative.

REFERENCES

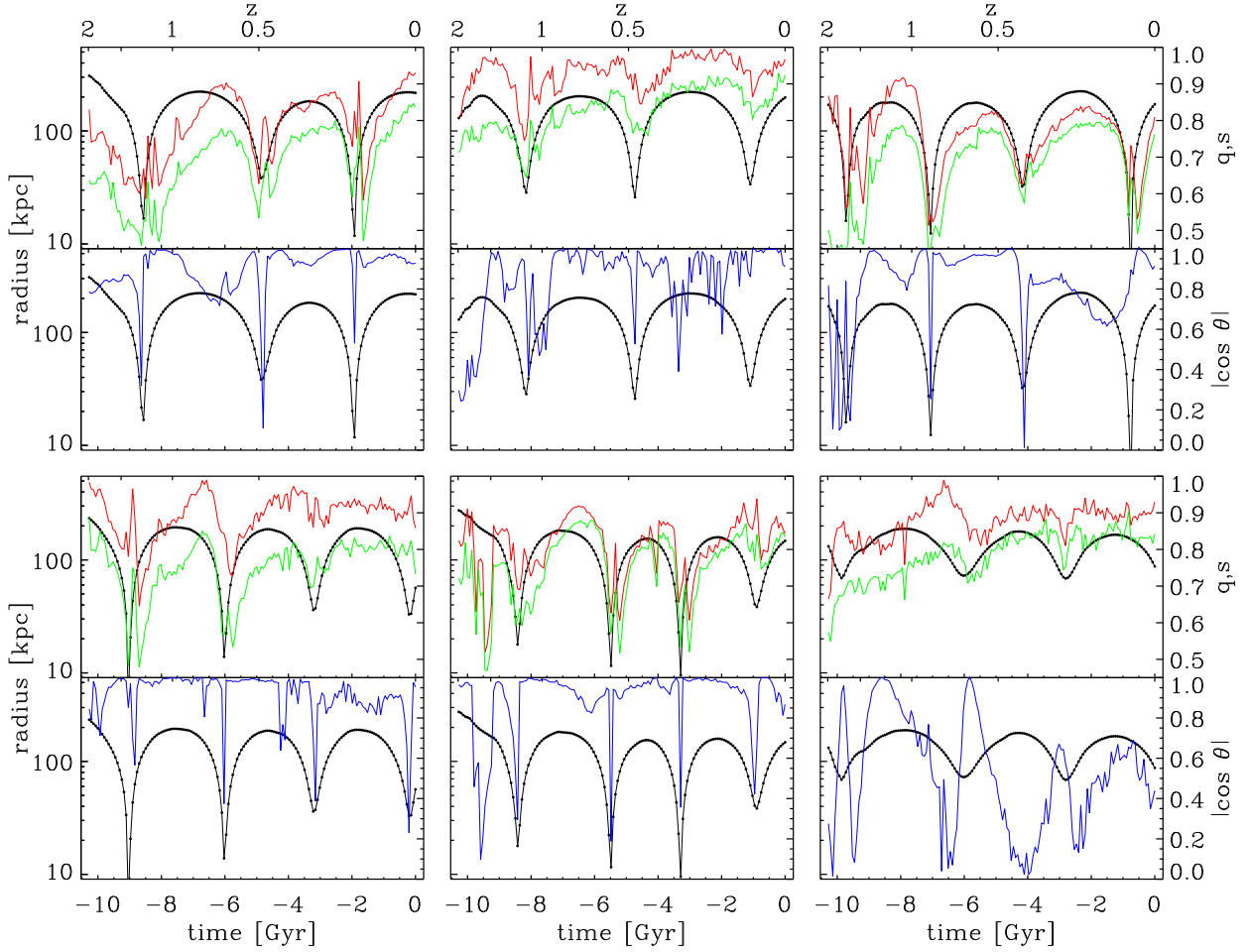


FIG. 11.— The shape parameters (measured within r_t) and alignment of six subhalos (see text for a discussion of their selection) as a function of time. In each plot the subhalo’s proper distance from the host halo is shown in the black solid line. For each subhalo the top panel also shows q (upper line, red) and s (lower line, green) and in the bottom panel $|\cos \theta|$, the angle between the subhalo’s major axis and the direction towards the halo center.

- Bacon, D. J., Massey, R. J., Refregier, A. R., & Ellis, R. S. 2003, MNRAS, 344, 673
- Bailin, J., Steinmetz, M., 2005, ApJ, 627, 647
- Barnes, J., & Efstathiou, G. 1987, ApJ, 319, 575
- Bertschinger, E. 2001, ApJS, 137, 1
- Bett, P., Eke, V., Frenk, C. S., Jenkins, A., Helly, J., & Navarro, J. 2007, MNRAS, 376, 215
- Brainerd, T. G. 2004, AIP Conf. Proc. 743: The New Cosmology: Conference on Strings and Cosmology, 743, 129
- Bridle, S., & King, L. 2007, in the “Gravitational Lensing” Focus Issue of the New Journal of Physics (astro-ph/0705.0166)
- Brown, M. L., Taylor, A. N., Bacon, D. J., Gray, M. E., Dye, S., Meisenheimer, K., & Wolf, C. 2003, MNRAS, 341, 100
- Bullock, J. S. 2002, in “The Shapes of Galaxies and Their Dark Matter Halos”, ed. P. Natarajan (Singapore: World Scientific), p. 109
- Ciotti, L., & Dutta, S. N. 1994, MNRAS, 270, 390
- Davis, M., Efstathiou, G., Frenk, C. S., & White, S. D. M. 1985, ApJ, 292, 371
- Diemand, J., Moore, B., & Stadel, J. 2004, MNRAS, 353, 624
- Diemand, J., Kuhlen, M., & Madau, P. 2007, ApJ, in press (astro-ph/0603250), paper I
- Diemand, J., Kuhlen, M., & Madau, P. 2007, submitted to ApJ (astro-ph/0703337), paper II
- Dubinski, J., & Carlberg, R. G. 1991, ApJ, 378, 496
- Dubinski, J. 1994, ApJ, 431, 617
- Efstathiou, G., Frenk, C. S., White, S. D. M., & Davis, M. 1988, MNRAS, 235, 715
- Faltenbacher, A., & Diemand, J. 2006, MNRAS, 369, 1698
- Faltenbacher, A., Li, C., Mao, S., van den Bosch, F. C., Yang, X., Jing, Y. P., Pasquali, A., & Mo, H. J. 2007, submitted to ApJ (astro-ph/0704.0674)
- Franx, M., Illingworth, G., de Zeeuw, T., 1991, ApJ, 383, 112
- Frenk, C. S., White, S. D. M., Efstathiou, G., & Davis, M. 1985, Nature, 317, 595
- Frenk, C. S., White, S. D. M., Davis, M., & Efstathiou, G. 1988, ApJ, 327, 507
- Gilmore, G., Wilkinson, M. I., Wyse, R. F. G., Kleyna, J. T., Koch, A., & Wyn Evans, N. 2007, ApJ, in press (astro-ph/0703308)
- Hamana, T., et al. 2003, ApJ, 597, 98
- Hayashi, E., Navarro, J., & Springel, V. 2007, MNRAS, in print (astro-ph/0612327)
- Helmi, A., 2004, ApJL, 610, L97
- Hirata, C. M., & Seljak, U. 2004, Phys. Rev. D, 70, 063526
- Hoekstra, H., et al. 2006, ApJ, 647, 116
- Hopkins, P. F., Bahcall, N. A., & Bode, P. 2005, ApJ, 618, 1
- Ibata, R., Lewis, G. F., Irwin, M., Totten, E., Quinn, T., 2001, ApJ, 551, 294
- Jarvis, M., Bernstein, G. M., Fischer, P., Smith, D., Jain, B., Tyson, J. A., & Wittman, D. 2003, AJ, 125, 1014
- Jing, Y. P., Mo, H. J., Borner, G., & Fang, L. Z. 1995, MNRAS, 276, 417

- Jing, Y. P., & Suto, Y. 2002, *ApJ*, 574, 538
- Kang, X., van den Bosch, F. C., Yang, X., Mao, S., Mo, H. J., Li, C., & Jing, Y. P. 2007, *MNRAS*, in print (astro-ph/0701130)
- Kasun, S. F., & Evrard, A. E. 2005, *ApJ*, 629, 781
- Katz, N. 1991, *ApJ*, 368, 325
- Katz, N., & White, S. D. M., 1993, *ApJ*, 412, 455
- Kazantzidis, S., Kravtsov, A. V., Zentner, A. R., Allgood, B., Nagai, D., Moore, B., 2004, *ApJL*, 611, L73
- Klypin, A., Kravtsov, A. V., Valenzuela, O., & Prada, F. 1999, *ApJ*, 522, 82
- Law, D. R., Johnston, K. V., Majewski, S. R., 2005, *ApJ*, 619, 807
- Lee, J., Kang, X., & Jing, Y. P. 2005, *ApJL*, 629, L5
- Libeskind, N. I., Frenk, C. S., Cole, S., Helly, J. C., Jenkins, A., Navarro, J. F., & Power, C. 2005, *MNRAS*, 363, 146
- Libeskind, N. I., Cole, S., Frenk, C. S., Okamoto, T., & Jenkins, A. 2007, *MNRAS*, 374, 16
- Lokas, E. L., Mamon, G. A., & Prada, F. 2005, *MNRAS*, 363, 918
- Macciò, A. V., Dutton, A. A., van den Bosch, F. C., Moore, B., Potter, D., & Stadel, J. 2007, *MNRAS*, in print (astro-ph/0608157)
- Majewski, S. R., Skrutskie, M. F., Weinberg, M. D., Ostheimer, J. C., 2003, *ApJ*, 599, 1082
- Mandelbaum, R., Seljak, U., Cool, R. J., Blanton, M., Hirata, C. M., & Brinkmann, J. 2006, *MNRAS*, 372, 758
- Mandelbaum, R., Hirata, C. M., Ishak, M., Seljak, U., & Brinkmann, J. 2006, *MNRAS*, 367, 611
- Martínez-Delgado, D., Gómez-Flechoso, M. Á., Aparicio, A., Carrera, R., 2004, *ApJ*, 601, 242
- Massey, R., et al., 2007, *ApJS*, in print (astro-ph/0701480)
- Moore, B., Ghigna, S., Governato, F., Lake, G., Quinn, T., Stadel, J., & Tozzi, P. 1999, *ApJL*, 524, L19
- Muñoz, R. R., et al. 2005, *ApJ*, 631, L137
- Nagai, D., & Kravtsov, A. V. 2005, *ApJ*, 618, 557
- Olling, R. P., Merrifield, M. R., 2000, *MNRAS*, 311, 361
- Quinn, P. J., Salmon, J. K., & Zurek, W. H. 1986, *Nature*, 322, 329
- Ragone-Figueroa, C., & Plionis, M., 2007, *MNRAS*, in print (astro-ph/0703440)
- Springel, V., White, S. D. M., & Hernquist, L. 2004, “The shapes of simulated dark matter halos”, in Ryder, S., Pisano, D., Walker, M., Freeman, K., eds, *IAU Symposium*, p. 241
- Strigari, L. E., Bullock, J. S., Kaplinghat, M., Diemand, J., Kuhlen, M., Madau, P., 2007, submitted to *ApJ* (astro-ph/0704.1817)
- Thomas, P. A., et al. 1998, *MNRAS*, 296, 1061
- Tormen, G. 1997, *MNRAS*, 290, 411
- Walker, M. G., Mateo, M., Olszewski, E. W., Bernstein, R., Wang, X., & Woodroffe, M. 2006, *AJ*, 131, 2114
- Warren, M. S., Quinn, P. J., Salmon, J. K., & Zurek, W. H. 1992, *ApJ*, 399, 405
- Wilkinson, M. I., Kleyna, J. T., Evans, N. W., Gilmore, G. F., Irwin, M. J., & Grebel, E. K. 2004, *ApJ*, 611, L21
- Zentner, A. R., Kravtsov, A. V., Gnedin, O. Y., & Klypin, A. A. 2005, *ApJ*, 629, 219